JOURNAL OF CATALYSIS 52, 310–320 (1978)

Particle Size Distribution Function of Supported Metal Catalysts by X-ray Diffraction

P. GANESAN,† H. K. KUO,† A. SAAVEDRA,* AND R. J. DE ANGELIS†,[1]

† *Department of Metallurgical Engineering and Materials Science and Institute for Mining and Minerals Research, University of Kentucky, Lexington, Kentucky 40506, and* * *Instituto Militar de Engenharia, Pca. Gen. Tiburcio, ZC 20,000, Urca, Rio de Janeiro, Brazil*

Received April 26, 1977; revised November 9, 1977

An X-ray diffraction method which is capable of determining average particle size, microstrain, and the particle distribution function existing in crystalline materials is presented. The method is based on the analysis of a single X-ray diffraction profile. Results obtained on coprecipitated nickel oxide on alumina- and silica-supported catalytic materials indicate that appreciable strains exist. It is suggested that the strains present in NiO could be due to the pressure developed in the small particles to balance the surface tension forces and the distortion produced by the deformation of face-centered cubic structure into a rhombohedral form. The changes in particle size distributions observed during sintering determined from three catalytic materials provide evidence that particle growth takes place by atomic migration mechanism. In one material the particle growth during sintering appears to be controlled predominantly by crystallite migration and coalescence. The sintering behavior appears to be controlled by the extent of the bimodal character of the initial distribution function and the average particle size in the as-received condition.

INTRODUCTION

There are a number of experimental techniques available to characterize the average crystallite size and crystallite size distributions of metal-supported catalysts (*1*). Selective gas adsorption techniques give only the average crystallite size and require prior knowledge of adsorbate–metal surface interaction (*2*). Small-angle X-ray scattering has the practical difficulty that the micropores present in the supports also act as scattering centers and interfere with the scattering from metal crystallites. However, this difficulty has been effectively eliminated by filling the pores with a liquid of electron density equivalent to that of the support (*3*, *4*). Transmission electron microscopy is direct and therefore more reliable, but involves the tedious examination of many specimens in order to insure that the sample is a true representative of the bulk catalyst (*5*). Magnetic methods described in detail by Selwood (*6*) have been applied to some metals and alloys, e.g., Ni, CO, and Fe. X-Ray line-broadening investigations of supported catalysts have been limited to finding the average crystallite size from integral breadth or half-intensity breadth of a diffraction profile. A few investigations have been reported where the crystallite size distribution was determined; however in these studies the lattice strain contribution to the X-ray line broadening was neglected or assumed to be zero (*7*–*9*).

[1] To whom correspondence should be addressed.

0021-9517/78/0522-0310$02.00/0

The major objective of this work is to develop a reliable method to measure the particle size distribution function of a supported metal catalyst using X-ray diffraction profile shape analysis. Distribution data of this type are required to test the existing catalyst sintering models (*10, 11*). The existing method of analysis, following Warren and Averbach (*12*), requires two orders of the diffraction profile in order to separate the particle size and strain contributions to the broadening of the X-ray line. In the case of supported metal catalysts, due to the difficulty of making satisfactory intensity measurements on the higher order reflections, it is very difficult, if not impossible, to obtain two orders of a (hkl) profile. Having only one order of a profile necessitates use of the assumption that the lattice strains are zero in order to compute the particle size distribution function.

There has been considerable work reported on the structure and stability of small clusters of atoms which indicates that the most stable particle consists of tetrahedron units of atoms existing in a multiple twinned array (*13, 14*). This concept finds some experimental support from electron microscope observations made on some face-centered cubic metals which show images containing internal strain contrast, which has been interpreted as being a result of the existence of multiply twinned structures (*15, 16*). In view of this, it is clear that the strain contribution to X-ray line broadening could be significant if the particle sizes are reasonably large and the lattice strains are appreciable. Thus one has to be careful in making zero strain assumption when using X-ray diffraction profile shape analysis in investigations on small particles. In addition the measurements of strains are important if the correlation between the lattice strains and specific activity of nickel catalysts, which has been suggested to exist (*17*), is to be established.

In this paper an approximate method of determining the particle size distribution function from a single X-ray diffraction profile from a material containing strains is reported. In this method the zero strain assumption is not required. Results obtained on coprecipitated nickel oxide on alumina and silica indicate that the strains present are very significant and must be taken into account. This paper contains a description of the X-ray diffraction method developed for investigating catalyst-type materials along with preliminary results obtained on the unreduced catalysts. Previous work by Shephard (*8*) on the alumina-supported nickel–nickel oxide catalysts indicates that the crystallite size of the nickel in the reduced catalysts closely follows that of the corresponding oxide. Therefore it is expected that the results obtained on the unreduced catalysts will correlate with the particle size distribution functions existing in the reduced catalysts. Investigations to confirm this are currently underway.

THEORY

Single Profile Analysis Technique

The single diffraction profile technique is based on the work of Gangulee (*18*) and Mignot and Rondot (*19*). The Stokes corrected cosine coefficients (*20*) from a (hkl) diffraction profile are composed of two components, a size coefficient A_L^S and a microstrain or distortion coefficient A_L^D; their relationship can be expressed as:

$$A_L = A_L^S \cdot A_L^D, \qquad (1)$$

where A_L are the Stokes corrected cosine coefficients at a given L, and L is $n\delta$. Here n is the harmonic number and δ is a distance normal to the diffracting planes. Defining a variable $X = 1/D_e$, where D_e is the effective diffracting particle size; for small values of n and δ where the values of L are small and such that the number of diffracting domains in the specimen with

this dimension is insignificant, the particle size term of the Fourier coefficients can be expanded as:

$$A_L^S = (1 - LX). \tag{2}$$

The distortion coefficients can be expanded for small values of n, as:

$$A_L^D = (1 - KL^2\langle\epsilon_L^2\rangle), \tag{3}$$

where K is $2\pi^2/d^2$, d is the (hkl) planar spacing, and $\langle\epsilon_L^2\rangle$ is the mean square of the microstrain averaged over all distances in the diffracting specimen spaced L apart.

Letting $Y_L = K\langle\epsilon_L^2\rangle$, the small L value cosine coefficient can be written as:

$$A_L = (1 - LX)(1 - Y_L L^2). \tag{4}$$

Equation (4) can be solved for X if the functional form of Y_L is known. In this way the particle size can be separated from the microstrain terms. The problem then resolves to determination of the most suitable forms of Y_L. Assuming the form of the strain function to be (*21*)

$$Y_L = (C/L)\delta K \tag{5}$$

leads to an expression for A_L of

$$A_L = 1 - L(X + C\delta K) + L^2(XC\delta K). \tag{6}$$

The expression for A_L has the form of a second-order polynomial in L. Now defining a polynomial of second degree:

$$R_L = a_0 + a_1 L + a_2 L^2, \tag{7}$$

the coefficients of which, by comparing with Eq. (6), are:

$$a_0 = 1; \quad a_1 = -(X + C\delta K); \quad \text{and} \quad a_2 = XC\delta K. \tag{8}$$

From these relations it follows that

$$\begin{aligned} X &= \tfrac{1}{2}(-a_1 \pm (a_1^2 - 4a_2)^{\frac{1}{2}}), \\ D_e &= 1/X, \\ C &= a_2/X\delta K, \\ \langle\epsilon_L^2\rangle &= (C/L)\delta. \end{aligned} \tag{9}$$

The determination of the coefficients a_0, a_1, and a_2 can be made by solving the system of equations:

$$\begin{aligned} \sum_t A_L &= a_0 N + a_1 \sum_t L + a_2 \sum_t L^2, \\ \sum_t LA_L &= a_0 \sum_t L + a_1 \sum_t L^2 + a_2 \sum_t L^3, \\ \sum_t L^2 A_L &= a_0 \sum_t L^2 + a_1 \sum_t L^3 + a_2 \sum_t L^4, \end{aligned} \tag{10}$$

where N is the number of coefficients used in the evaluation, $N \geq 4$; t is an integer satisfying $t = (L_N - L_0)/(L_1 - L_0)$, where L_0 is the distance corresponding to the initial coefficient used in the computation of Eq. (10).

The best solutions to Eq. (10) are selected from four criteria: (i) $a_0 \approx 1$; (ii) $a_2 > 0$, since a_2 from Eqs. (6) and (7) can be written as d^2A_L/dL^2 which must be positive; (iii) $\sum_t (R_L - A_L)/N$ is a minimum; (iv) $(dA_L/dL)_{L\to 0} = a_1 = -(X + C\delta K)$. After the best solution to Eq. (10) is determined it is a simple process to calculate the average coherent diffracting particle size D_e and lattice mean square strain $\langle\epsilon_L^2\rangle$ by employing Eq. (9).

Particle Size Distribution Function

While single profile analysis provides a convenient method to calculate lattice microstrain it is important to note that the particle size distribution function cannot be obtained by this method alone, since from Eq. (2), $d^2A_L^S/dL^2$ reduces to zero. However by employing the usually accepted small (L/d) approximation it is possible to obtain the particle size distribution function by combining both single profile and multiple order analysis as follows. Although this approach does contain limitations, it is a major improvement over the zero strain approximation.

The expression for the relationship between the particle size and distortion coefficients in the Warren–Averbach method (*12*) is given by

$$A_L = A_L^S\langle\cos 2\pi L/d\epsilon_L\rangle. \tag{11}$$

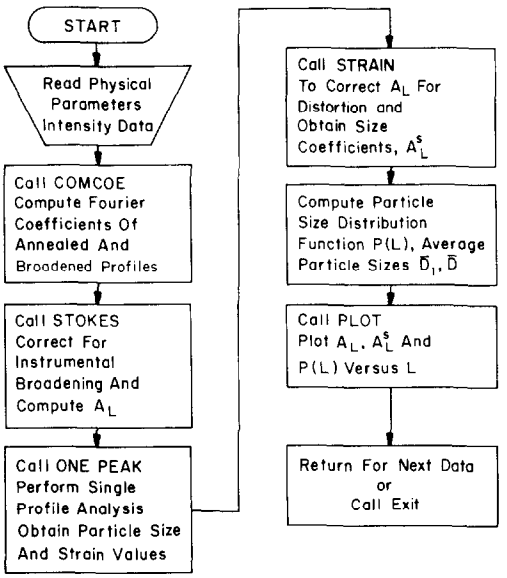

FIG. 1. Block diagram indicating the major elements of the computer program.

For small values of L/d the argument of the microstrain term is small and, using the approximations $\langle \cos X \rangle = 1 - \langle X^2 \rangle/2$ and $1 - X \simeq \exp(-X)$, Eq. (11) can be written as

$$A_L = A_L^S \exp -2\pi L^2/d^2\langle \epsilon_L^2 \rangle. \quad (12)$$

This method of separation of particle size and microstrain term makes no assumption of the nature of strains and Eq. (12) is good only for small values of L/d. However it can be shown (*22*) that Eq. (12) is exact for all values of L/d if the microstrain distribution is Gaussian. The distribution of strains at a given L has been shown to be close to Gaussian (*23–25*), but not the variation of $\langle \epsilon_L^2(\text{hkl}) \rangle^{\frac{1}{2}}$ with L.

Now it is possible to obtain the particle size coefficient A_L^S from Eq. (12) by substituting the values for mean square strain $\langle \epsilon_L^2 \rangle$ obtained from single profile analysis [Eq. (9)]. The particle size distribution function, $P(L)$, can then be obtained from the second derivative of A_L^S with respect to L (*22*), that is,

$$P(L) = \frac{d^2 A_L^S}{dL^2} \cdot \text{De}. \quad (13)$$

The particle size distribution data can be employed to calculate the average particle size using two relationships:

$$\bar{D} = \sum_L LP(L)\Delta L \quad (14a)$$

$$\bar{D}_1 = \left[\sum_L \frac{1}{L} P(L)\Delta L \right]^{-1}, \quad (14b)$$

where $P(L)$ is the value of the distribution function at the size L normalized such that $\int P(L)dL = 1$. $\bar{D}$ is the volumetric mean particle size and $\bar{D}_1$ is the average value of the thickness of the particle normal to the (hkl) reflecting planes (*26*).

The complete X-ray diffraction profile shape analysis which involves the calculation of Stokes corrected coefficients A_L, particle size coefficients A_L^S, and particle size distribution function $P(L)$ has been computerized. Figure 1 contains a schematic of the computer program.

EXPERIMENTAL

The description of the catalytic materials used in this investigation, which were supplied by Catalysts and Chemicals Inc., is given in Table 1. Pellets of the four unreduced catalysts were ground into powders and were pressed at 40,000 psi into pellets of 1.25 in. diameter and approximately 0.25 in. thick.

A Picker diffractometer and a Cu-target x-ray tube were used for the diffraction runs. A diffracted beam monochromator was constructed employing a single bent grain oriented graphite monochromator crystal. This eliminated most of the background intensity outside the diffraction lines. A proportional detector with pulse height analyzer was used for the detection system.

X-Ray data describing the X-ray diffraction profile from the four unreduced catalysts were collected in the as-received condition and after sintering for 1 hr at 900 or 1000°C. Due to extremely small

TABLE 1

Physical and Chemical Properties of Catalytic Materials

	Catalyst No.			
	C-150-1-01	C-150-1-02	C-150-1-03	C-150-4-03
Ni (%)	51.7	46.6	47.0	55.6
C (%)	2.94	2.13	5.84	2.70
Cl (%)	—	—	0.006	0.013
S (%)	0.06	0.04	0.09	0.09
Surface area (m^2/g)	211	301	202	177
Pore volume (cm^3/g)	0.34	0.58	0.328	0.514
Density (g/cm^3)	1.05	0.88	1.01	0.93

particle sizes of the catalysts in the as-received condition (25 to 40 Å) the tails of the (111), (200), (222), and (400) profiles of NiO overlapped with a neighboring profile. Hence data on the (220) profile from the unreduced catalysts were collected. In addition, NiO is rhombohedral at room temperature and the (220) line is a single line. The data were collected by step scanning in 1/30 degree steps counting 500 seconds per step. The standard used to correct the data for instrumental broadening was a pure chemical-grade NiO which was sintered in the pellet form for 4 hr at 1300°C.

RESULTS

There are several methods to characterize the crystallite size by X-ray diffraction. The simplest is the determination of the effective particle dimension from the half-breadth of the profile, $D_{\text{half-breadth}}$, by the Scherrer formula

$$D_{\text{half-breadth}} = K\lambda/\beta_D \cos\theta, \qquad (15)$$

where β_D is the half-breadth of the profile corrected for instrumental broadening, λ is the wavelength, θ is the diffraction angle, and K is a constant close to 0.9.

The particle size can also be determined from the initial slope of the Stokes corrected coefficients (in this method the strains in the material are assumed to be zero). In this case the particle size is given by (*28*):

$$D_{\text{coefficient}} = [-(dA_L/dL)_{L\to 0}]^{-1}. \qquad (16)$$

The strain-corrected effective particle size obtained employing the single profile analysis technique [Eq. (9)] has been designated as $D_{\text{one peak}}$. The NiO particle sizes in catalytic materials determined by the above methods, together with the values of $\bar{D}_1$, $\bar{D}$, and $D_{\max}$ determined from particle size distribution as defined earlier, are reported in Table 2.

The particle sizes determined from the half-breadth of the diffraction profile are from 1.50 to 2.0 times greater than those obtained from the coefficients (D coefficient), single-peak analysis, and D one peak, and the distribution function ($\bar{D}_1$ and $\bar{D}$) reflects the extent of the approximations involved in the half-breadth approach. The accuracy with which the Scherrer equation can be applied is limited by the uncertainties in K and the size distribution effects in modifying the breadth and shape of a diffraction line. For these reasons Klug and Alexander (*29*) point out that the effective diameter obtained by this method may have an absolute accuracy of only 50%. As expected the $\bar{D}_1$ particle size values are always smaller than $\bar{D}$ and the ratio of $\bar{D}_1/D$ decreases as the particle size distribution function becomes broader (*26*).

TABLE 2

Particle Sizes and Microstrains of Nickel Oxide Catalyst Materials as Measured by Various X-Ray Diffraction Techniques

Catalyst No.	$D_{\text{half-breadth}}$[a] (Å)	$D_{\text{coefficient}}$[b] (Å)	$D_{\text{one peak}}$[c] (Å)	$\bar{D}_1$[d] (Å)	$\bar{D}$[e] (Å)	$D_{\max}$[f] (Å)	Microstrain ($\langle \epsilon^2 \, 20 \text{ Å} \rangle^{\frac{1}{2}} \times 10^2$)
C-150-1-01 Silica[g]	28.8	20.8	20.4	17.6	18.3	18.0	0.40
C-150-1-02 Silica[g]	37.3	21.0	22.0	19.7	21.3	18.0	0.60
C-150-1-03 Alumina[g]	24.5	18.4	19.5	17.9	20.0	16.0	0.57
C-150-4-03 Alumina[g]	38.5	24.5	25.8	22.9	25.6	21.0	0.77
C-150-1-01 (1000°C, 1 hr)[h]	96.1	54.0	48.0	45.1	62.2	48.0	0.23
C-150-1-02 (1000°C, 1 hr)[h]	67.1	46.0	50.0	41.6	53.4	44.0	0.32
C-150-1-03 (1000°C, 1 hr)[h]	120.8	78.0	72.0	72.3	92.5	50.0	0.39
C-150-4-03 (500°C, 1 hr)[h]	39.8	26.0	26.0	25.9	27.6	26.0	0.72
C-150-4-03 (900°C, 1 hr)[h]	151.3	91.0	88.5	69.9	93.0	80.0	0.19
C-150-4-03 (1000°C, 1 hr)[h]	181.7	103.0	103.8	99.5	127.3	110.0	0.36

[a] Effective particle size from half-breadth of the profile by Scherrer formula [Eq. (15)].
[b] Particle size from the initial slope of the Stokes corrected coefficients [Eq. (16)].
[c] Effective particle size from single profile analysis technique [Eq. (9)].
[d] $\bar{D}_1 = [\sum_L (1/L) P(L) \, \Delta L]^{-1}$.
[e] $\bar{D} = \sum_L L \, P(L) \, \Delta L$.
[f] $D_{\max}$ is the value of the crystallite size having maximum probability.
[g] Support.
[h] Heat treatment.

Attempts at the independent determination of the average particle size of the unreduced catalyst form by chemisorption are not possible because hydrogen does not adsorb on nickel oxide. However, the particle sizes obtained by the X-ray diffraction technique on reduced nickel catalysts were found to agree very well with those obtained from the surface area measurements by hydrogen chemisorption (*27*).

The particle size distribution functions obtained from the C-150-4-03 (alumina supported) unreduced catalyst in the as-received and sintered conditions are shown in Fig. 2. These data indicate that sintering at 900 and 1000°C causes nickel oxide particles to grow rapidly and also produces a broadening of particle size distribution. The effect of sintering at 500°C in terms of particle growth is small but the particle size distribution becomes sharper. The same data are plotted in Fig. 3 with the particle size normalized by dividing it by $D_{\max}$, the value of the crystallite size having maximum probability density. The evidence of the formation of particles smaller than the initial minimum particle size is more apparent in Fig. 3 as compared to Fig. 2. Figures 4–6 show similar plots for catalysts C-150-1-01, C-150-1-02, and C-150-1-03.

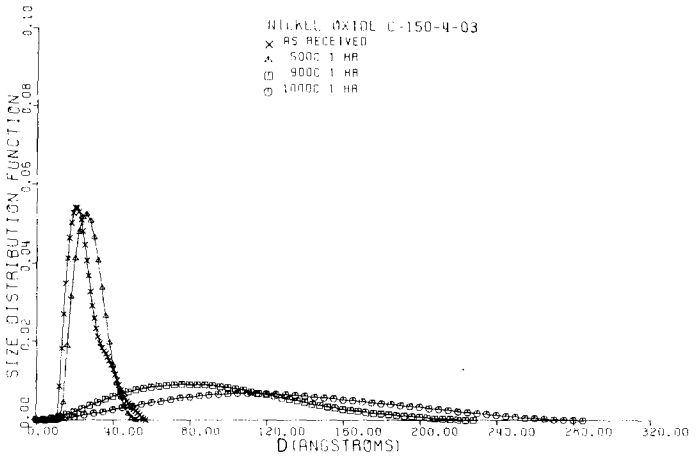

FIG. 2. Particle size distribution functions of as-received and sintered NiO catalyst C-150-4-03.

The values of the lattice microstrain existing in the unreduced catalysts in the as-received and sintered conditions, obtained by the single profile analysis method, are reported in Table 2. These results indicate that the strains present in the supported metal catalysts are of significant magnitude and the strains tend to decrease upon sintering.

The effect of zero strain assumption on the size distribution function was evaluated by determining the distribution functions from both A_L and A_L^S. The difference between these are clearly demonstrated in Figs. 7 and 8. In the sintered condition, even though the strains are lower (see Table 2) when compared to the as-received sample, the effect of the microstrain on the X-ray line broadening and hence on the size distribution function is more pronounced.

DISCUSSION

The particle size distribution functions obtained for these catalysts are comparable to those obtained for similar catalysts by others (*8*, *30*, *31*). The observed particle size distribution functions are generally

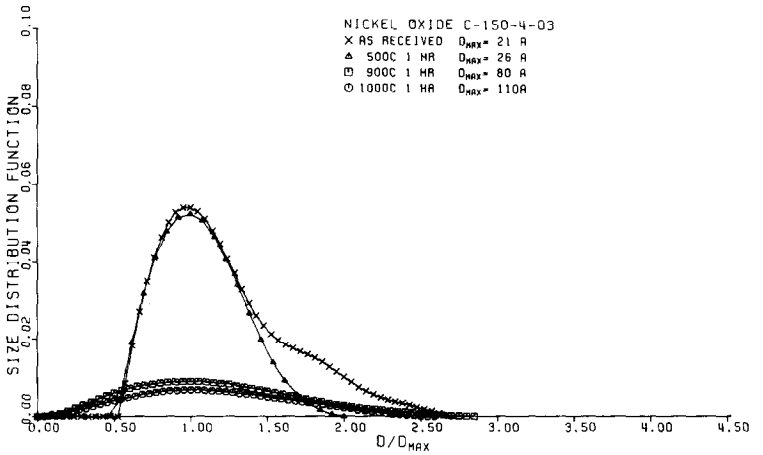

FIG. 3. Particle size distribution functions of as-received and sintered NiO catalyst C-150-4-03 normalized by dividing D by D_{max}. The values of D_{max} are indicated.

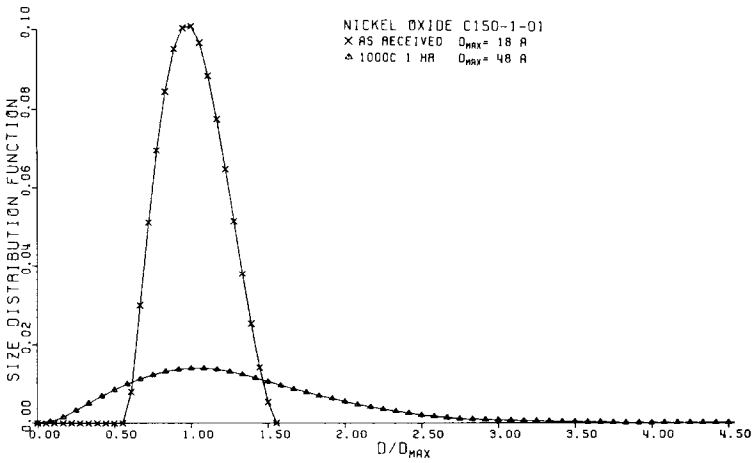

FIG. 4. Particle size distribution functions of as-received and sintered NiO catalyst C-150-1-01 normalized by dividing D by D_{max}. The values of D_{max} are indicated.

consistent with both the atomic migration (*11*) and the particle coalescence models (*32*) of sintering. Because the two models predict many similar changes in the particle size distribution functions it has been difficult to obtain unambiguous data characteristic of one particular model. For instance the development of the tails on the large diameter side of the distribution function can be reconciled with both models (*33, 34*). However, the formation of a significant tail in the particle size distribution function in the small particle size range (e.g., see Figs. 3–5) suggests strongly that the atomic migration mechanism is operating (*11*). All of the changes in particle size distribution functions observed on all catalysts, except on C-150-1-03, provide evidence that the atomic migration mechanism is operative.

The behavior of the particle size distribution function in C-150-1-03 catalyst appears to indicate that a coalescence mechanism was operative. The pronounced bimodal character of the distribution function and the initial smaller particle size of the as-

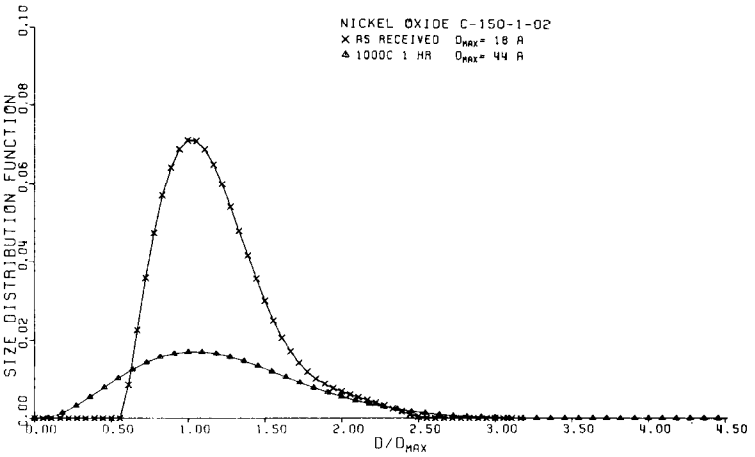

FIG. 5. Particle size distribution functions of as-received and sintered NiO catalyst C-150-1-02 normalized by dividing D by D_{max}. The values of D_{max} are indicated.

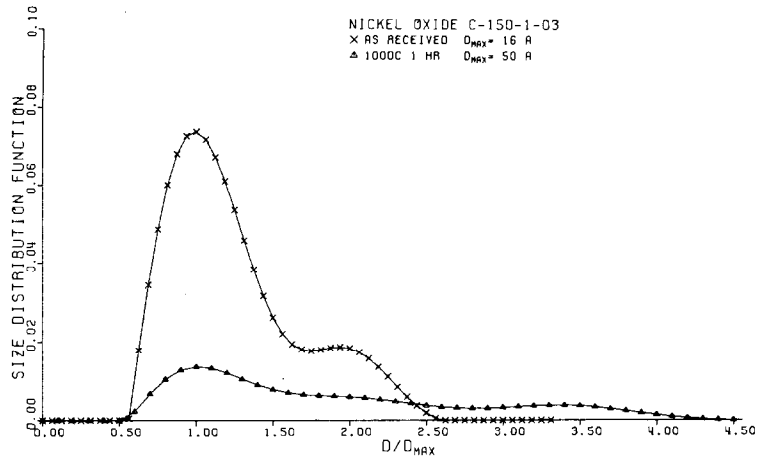

FIG. 6. Particle size distribution functions of as-received and sintered NiO catalyst C-150-1-03 normalized by dividing D by D_{max}. The values of D_{max} are indicated.

received material would tend to promote particle growth by coalescence as suggested by Wynblatt and Gjostein (*35*). This is also consistent with the behavior of alumina-supported nickel catalysts reported by Richardson and Desai (*30*). Assuming the particle growth by coalescence to predominate, the bimodal character would tend to be preserved during sintering as observed for this case.

In the case of C-150-4-03 catalyst the particle size is substantially larger in the as-received material. This would tend to inhibit coalescence and favor atomic migration. The sintering behavior of this catalyst has all the characteristics associated with the atomic migration mechanism. The fact that the low-temperature sintering of this material produces a sharper distribution is rather interesting and needs further investigation. If this phenomenon occurs generally, then low-temperature pretreatment of the catalyst prior to reduction could reduce the rate of sintering after the catalyst has been put into service in methanation.

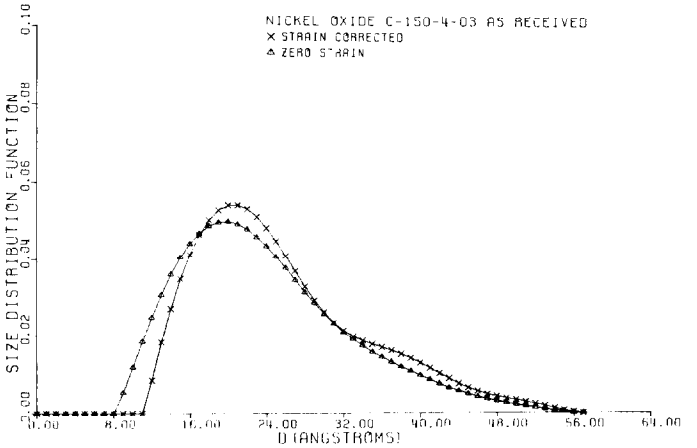

FIG. 7. The particle size distribution functions in the as-received NiO catalyst C-150-4-03 obtained using the zero strain and strain-corrected conditions.

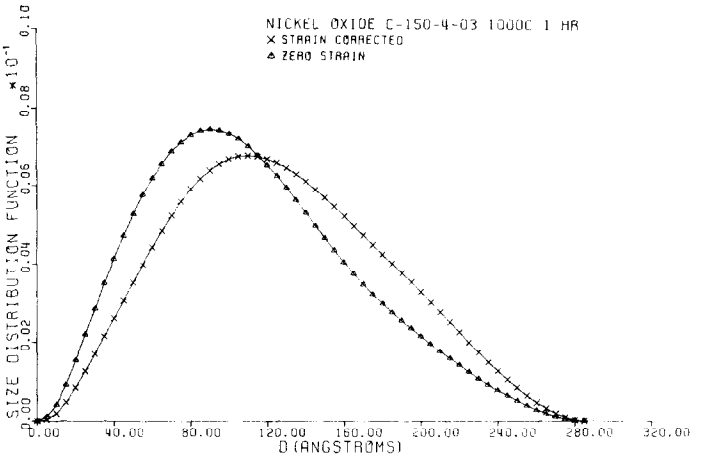

FIG. 8. The particle size distribution functions in the NiO catalyst C-150-4-03, sintered at 1000°C for 1 hr, obtained using the zero strain and strain-corrected conditions.

The presence of large lattice strains in nickel oxide brings out the importance of separating the strain component of X-ray line broadening because it could be an important consideration in catalysis activity and, by assuming the strains to be zero, could lead to as high as a 25% error in the estimation of average particle size. While it is difficult to pinpoint the reason for the presence of microstrains in these catalysts, several possibilities which could cause these strains will be given.

If the surface to volume ratio of small particles is very high, an internal pressure might develop in these particles which is inversely proportional to the particle radius. This pressure that develops to balance the surface tension forces would lead to the creation of internal strains. Based on a minimum energy configuration Hoare and Pal (*13*) have shown that certain nonlattice growth schemes showing tetrahedral, pentagonal, and icosahedral symmetry are appreciably more stable than microcrystallites based on face-centered cubic (fcc) structures. Allpress and Sanders (*14*) have shown that, if complex structures such as those mentioned above were formed from units of a regular tetrahedron with an undistorted fcc structure bounded by (111) faces, the complete particles would contain gaps due to misfit between adjoining units. Electron microscope images of small particles (*16*, *36*) reveal no dislocations or faults but do show some strain contrast. These observations would indicate that the misfit is distributed throughout the particle by a relaxation of the fcc structure of each unit (*14*). Allpress and Sanders (*14*) have shown that the deviation from ideal fcc structure is more pronounced for decreasing particle size. This is attributed to the proportionally higher number of the surface atoms in small crystallites which have less than the maximum number, 12, of nearest neighbors. This would explain the decrease of strains upon sintering, since as the crystallite size increases the structure would tend to be more toward ideal face-centered cubic.

The strains present in NiO could also be due to the deformation of the face-centered cubic structure into a rhombohedral form as reported by Rooksby (*37*). At the present time we can only speculate that the strains present in these materials could be due to the pressure developed in the small particles to balance the surface tension forces and/or the distortion produced by rhombohedral deformation of

face-centered cubic structure. The reduction of strains upon sintering and the presence of an appreciable amount of strains even after sintering are consistent with either of these possibilities.

CONCLUSIONS

(i) By an extension of a diffraction method based on the analysis of a single X-ray line profile it is now possible to obtain the particle size distribution function corrected for strain broadening. (ii) The particle size distribution function of NiO-supported catalysts broadens upon sintering for 1 hr at 900 and 1000°C. The average particle size increases and there is evidence of formation of particles smaller than the initial minimum particle size. (iii) The mean square microstrains that exist in small NiO particles are appreciable and the strain correction has a greater effect on the particle size distribution function as the average particle size increases.

ACKNOWLEDGMENTS

This research was sponsored by the Institute for Mining and Minerals Research through Contract No. PD 18 and by the Energy Research and Development Agency through Contract No. E (49-18) 2229.

REFERENCES

1. Whyte, Jr., T. E., *Catal. Rev.* **8**, 117 (1973).
2. Muller, J., *Rev. Pure Appl. Chem.* **19**, 151 (1969).
3. Gunn, E. L., *J. Phys. Chem.* **62**, 928 (1958).
4. Whyte, Jr., T. E., Kirklin, P. W., Gould, R. W., and Heinemann, H., *J. Catal.* **25**, 407 (1972).
5. Adams, C. R., Benesi, H. A., Curtis, R. M., and Meisenherimer, R. G., *J. Catal.* **1**, 336 (1962).
6. Selwood, P. W., "Adsorption and Collective Paramagnetism," p. 46. Academic Press, New York, 1962.
7. Pausescu, P., Manaila, R., and Popescu, M., *J. Appl. Crystallogr.*, **7**, 281 (1974).
8. Shephard, F. E., *J. Catal.* **14**, 148 (1969).
9. Coenen, J. W. E., and Linsen, B. G., "Physical and Chemical Aspects of Adsorbents and Catalysts," (B. G. Linsen, Ed.), p. 471. Academic Press, London, 1970.
10. Ruckenstein, E., and Pulvermacher, B., *AIChE J.* **19**, 224, 356 (1973).
11. Flynn, P. C., and Wanke, S. E., *J. Catal.* **34**, 390, 400 (1974).
12. Warren, B. E., and Averbach, B. L., *J. Appl. Phys.* **21**, 595 (1950).
13. Hoare, M. R., and Pal, P., *Advan. Phys.* **20**, 161 (1971).
14. Allpress, J. G., and Sanders, J. V., *Aust. J. Phys.* **23**, 23 (1970).
15. Ino, S., *J. Phys. Soc. Japan* **21**, 346 (1966).
16. Kimoto, K., and Nishida, I., *J. Phys. Soc. Japan*, **22**, 940 (1967).
17. Kishimoto, S., *J. Phys. Chem.* **77**, 1719 (1973).
18. Gangulee, A., *J. Appl. Crystallogr.* **7**, 434 (1974).
19. Mignot, J., and Rondot, D., *Acta Met.* **23**, 1321 (1975).
20. Stokes, A. R., *Proc. Phys. Soc.* **61**, 382 (1948).
21. Rothman, R. L., and Cohen, J. B., *Advan. X-Ray Anal.* **12**, 208 (1969).
22. Warren, B. E., *Prog. Metal Phys.* **8**, 152 (1959).
23. McKeehan, M., and Warren, B. E., *J. Appl. Phys.* **24**, 52 (1953).
24. Evans, W. P., Ricklefs, R. E., and Millan, J. F., *in* "Local Atomic Arrangements Studied by X-ray Diffractions" (J. B. Cohen and J. E, Hilliard, Eds.), p. 351. Gordon and Breach. New York, 1966.
25. De Angelis, R. J., *in* "Local Atomic Arrangements Studied by X-ray Diffraction" (J. B. Cohen and J. E. Hilliard, Eds.), p. 271. Gordon and Breach, New York, 1966.
26. Guinier, A., "X-ray Diffraction in Crystals, Imperfect Crystals and Amorphous Bodies." Freeman, San Francisco, 1963.
27. Lin, C. H., M. S. Thesis, University of Kentucky, May, 1977.
28. Bertaut, E., *in* "International Tables for X-ray Crystallography" (C. H. Macgillavry and G. D. Rieck, Eds.), Vol. 3, p. 318. The Kynoch Press, Birmingham, England, 1962.
29. Klug, H. P., and Alexander, L. E., "X-ray Diffraction Procedures." Wiley, New York, 1967.
30. Richardson, J. T., and Desai, P., *J. Catal.* **42**, 294 (1976).
31. Sashital, S. R., Burwell, R. L., Jr., Butt, J. B., and Cohen, J. B., to be published.
32. Granquist, C. G., and Buhrman, R. A., *J. Catal.* **42**, 477 (1976).
33. Wanke, S. E., *J. Catal.* **46**, 234 (1977).
34. Granquist, C. G., and Burhman, R. A., *J. Catal.* **46**, 238 (1977).
35. Wynblatt, P., and Gjostein, N. A., *Progr. Solid State Chem.* **9**, 21 (1975).
36. Komoda, T., *Japan. J. Appl. Phys.* **7**, 27 (1968).
37. Rooksby, H. P., *Acta Crystallogr.* **1**, 226 (1948).